Energy Storage Materials 63 (2023) 103029

Contents lists available at ScienceDirect

Energy Storage Materials

journal homepage: www.elsevier.com/locate/ensm

Single-ion conducting interlayers for improved lithium metal plating

Jiajia Wan [a], Xu Liu [b,c], Thomas Diemant [b,c], Mintao Wan [b,c], Stefano Passerini [b,c,d], Elie Paillard [e,*]

[a] Politecnico di Milano, Chemistry Department, via Lambruschini 4, 20148 Milan, Italy
[b] Helmholtz Institute Ulm, Helmholtzstraße 11, D-89081 Ulm, Germany
[c] Karlsruhe Institute of Technology (KIT), P.O. Box 3640, D-76021 Karlsruhe, Germany
[d] Sapienza University of Rome, Chemistry Department, Piazzale A. Moro 5, I-00185 Rome, Italy
[e] Politecnico di Milano, Energy Department, via Lambruschini 4, 20148 Milan, Italy

ARTICLE INFO

Keywords:
Li metal batteries
Artificial SEI
Single-ion conductors
Dendrites

ABSTRACT

Li metal batteries have attracted much attention due to their superior theoretical capacity with respect to conventional Li-ion batteries. However, safety issues caused by inhomogeneous stripping/plating and serious dendrite growth greatly limit their commercial application. Herein, we report on the preparation of single-ion conducting artificial solid electrolyte interphases (art-SEIs) on the surface of Li metal, to improve lithium metal confinement and current density homogeneity, while limiting lithium depletion at the Li/electrolyte interface during charge. Considerable improvements in terms of the Li anode life cycle are reported by combining the art-SEIs and liquid ether electrolytes, although the use of liquid electrolytes and separators still limits the anode performance. Finally, the combined use of a polyethylene oxide single-ion conducting solid polymer electrolyte and the stiff and ionically concentrated single-ion art-SEI enables Li metal long-term cycling.

1. Introduction

Li-metal batteries have the potential to provide an increased energy density vs. Li-ion batteries and thereby play a significant role in the energy transition requiring improved energy storage systems for electric transportation and stationary storage. However, the lithium metal anode remains challenging due to the inhomogeneous deposition of lithium during cycling. Several methods have been proposed to improve the homogeneity of lithium plating and stripping. One approach consists in addressing lithium transport in the electrolyte, via increasing the lithium transference number up to the use of single-ion conductors [1–4]. However, inhomogeneous plating occurs much before the lithium concentration decreases significantly at the anode. This is caused by the inhomogeneity of the local current density and insufficient confinement of the lithium metal anode. This is linked, on the one hand, to the use of separators combined with liquid electrolytes that induce inhomogeneous pressure and current densities. On the other hand, the solid electrolyte interphase (SEI) plays a significant role in the homogeneity of the plating, since it affects the homogeneity of the local current density and of the applied pressure[5]. In addition, as inhomogeneous plating occurs, it evolves, via stretching, cracking, and self-repair, which is a source of further inhomogeneities.

Thus, the strategy of fabricating artificial SEI (art-SEI) ex-situ has been used to improve lithium metal confinement and improve the homogeneity of the current density [6–9]. In this regard, some inorganic compounds such as LiF, Li_3PO_4, Li_3N, and amorphous Al_2O_3 were proposed as effective art-SEIs layers to enable more uniform Li deposition and restrain Li dendrite growth [10–16]. However, the intrinsic brittleness of these materials used as protective layers limits the long-term cycling of Li metal batteries since they cannot accommodate the huge lithium volume change during repeated plating/stripping processes and thus easily crack. Another strategy consists in coating an organic layer like functional organic salts, metal-organic frameworks, covalent organic frameworks, or ionic liquids on the surface of Li anode as a protective interface [17–21]. For example, Kang et al. prepared organic art-SEI layers using alcohols or carboxylic acids as reagents to decrease the interface resistance, prevent further electrolyte side reaction with fresh Li, reduce the initial deposition overpotential, and improve Li metal plating, thus leading to improved performance of Li||Li symmetrical cells and Li||NMC full cells [18,19]. Besides, polymers possessing the advantages of good mechanical stability, excellent flexibility, and high elasticity can be applied as art-SEI layer to achieve fast Li-ions

* Corresponding author.
E-mail address: elieelisee.paillard@polimi.it (E. Paillard).

https://doi.org/10.1016/j.ensm.2023.103029
Received 29 March 2023; Received in revised form 11 September 2023; Accepted 22 October 2023
Available online 29 October 2023

transportation and interface stability simultaneously [22–24]. Especially, the in-situ polymerization of monomers on the Li metal surface can greatly improve the compatibility of Li anode and polymer [25,26]. Furthermore, single-ion conducting polymers with high cationic transference numbers (t_{Li+} close to 1), are, a priori, superior to non-ionic polymer systems ($t_{Li+} < 0.4$) due to their potential to reduce the salt concentration gradients and thus significantly suppress the lithium dendrite growth [27,28]. For instance, Yu et al. proposed a dynamic single-ion-conductive network composed of tetrahedral $Al(OR)_4^-$ (R = soft fluorinated linker) centers serving as an art-SEI with considerable Li^+ conduction to reduce the interfacial resistance, achieve a rather homogeneous Li deposition and mitigate the parasitic reaction between the electrolyte and Li anode [29].

The properties of an ideal SEI, i.e., a single-ion conductor that only allows Li^+ transport and blocks other electrolyte species and electrons to prevent continuous electrolyte reactions, have been known for a while. However, the structure of the SEI is still under investigation. The very first representation showing a patchwork of various phases (i.e., Li_2CO_3, LiF, Li_2O, organic compounds, etc.) is still often found in the literature, and is shown in Fig. 1a but tends to be replaced by a bi-layered structure, shown in Fig. 1b. In this latter scheme, the 'outer layer' of the SEI is composed of an accumulation of oligomeric organic degradation products that are partially reduced. Since this 'outer layer' is swollen by the electrolyte, it is described as 'gel-like'. In contrast, the SEI's 'inner layer' mainly consists of inorganic compounds originating from more extensive reduction reactions, which corresponds more closely to the 'ideal' SEI. It is up to debate whether the outer SEI is indeed an SEI since, in most cases, it is permeable to electrolytes species or can even be re-dissolved and redeposited during cycling (especially in the case of insertion anodes such as graphite) [30,31]. Art-SEI, as-deposited, are, on the one hand, a reagent to form the inner layer, while, depending on their affinity with electrolyte species, serve as an 'outer layer' swollen or not by electrolyte compounds.

In this regard, art-SEIs made of single-ion conducting polymers often have good affinity with the electrolyte. Thus, it remains questionable whether they fully maintain their single-ion conduction properties in presence of a liquid electrolyte. However, even though they may not fully suppress concentration gradients, they allow maintaining a minimal Li^+ concentration at the Li/electrolyte interface, thereby preventing full depletion, depending on the electrolyte uptake and the initial ionic concentration in the 'dry' (i.e., without solvent) art-SEI. In fact, it is known that for reaching high (single-ion) conduction, a 'dry' polymeric layer must incorporate ionic functions separated by solvating units and exhibit a high local segmental mobility. An issue though, for high conductivity polymer electrolytes (i.e., with high segmental mobility), is that conductivity is usually correlated with low mechanical properties. Thus art-SEIs must have properties that differ from polymer electrolytes, with a high Li^+ content, even at the cost of a low conductivity since the final 'dry' art-SEI inner layer is usually only few nm thick and the outer layer is plasticized by the electrolyte that provides solvating units.

Therefore, we propose herein the use of water-stable single-ion conducting polymeric layers with a perfluorinated bis(sulfonyl)imide anionic function every repeating unit. Two types of polymeric backbones were tested and combined to tune the affinity with the electrolyte. Thereby, beside differences in terms of reactivity with Li metal upon application of the art-SEI, we can expect a different balance between conductivity, t_{Li+} and mechanical properties depending on the polymer or polymer mixture used.

The combined use of a single-ion solid polymer electrolyte (SISPE) and art-SEIs is *a priori* the most robust approach for tackling homogeneous lithium deposition in lithium metal batteries. However, the use of solid electrolytes prevents, for the most part, the systematic study of art-SEIs. Indeed, on the one hand, the single-ion electrolytes affect the confinement of lithium metal by their mechanical strength, and on the other hand, cell disassembly is difficult and anode observation thereby often requires the use of tomographic techniques that are relatively low throughput and not readily available. Thus, we report here the improvements obtained via coating various art-SEIs in terms of Li metal anode's cyclability in liquid, ether-based electrolytes, and then the combination of polyethylene oxide (PEO)-based SISPE and art-SEI to showcase the strong improvement the latter brings via long term cycling of Li metal anodes.

2. Experimental section

2.1. Materials

Poly(lithium sulfonyl(trifluoromethanesulfonyl)imide styrene) (PSTFSILi, Specific Polymers) (M_n = 27,592 g mol^{-1}, M_w = 190,562 g mol^{-1}, I_p = 6.9 (GPC, eluent: DMF), poly(lithium sulfonyl(trifluoromethanesulfonyl)imide methacrylate) (PMTFSILi, Specific Polymers) (M_n = 208,828 g mol^{-1}, M_w = 356,953 g mol^{-1}, I_p = 1.7 (GPC, eluent: DMF), lithium bis(fluorosulfonyl)imide (LiFSI, Solvionic), 1,2-dimethoxyethane (DME, Merck), propylene carbonate (PC, Heliume Tech), 1-methyl-2-pyrrolidinone (NMP, Merck), Super C65 (Imerys), carbon coated $LiFePO_4$ (LFP, M23, Advanced Lithium Electrochemistry Co., Ltd.), lithium nickel cobalt manganese oxide ($LiNi_{0.8}Mn_{0.1}Co_{0.1}O_2$, NMC811, TMAX), poly(vinylidene difluoride) (PVDF, TMAX), poly (ethylene glycol) dimethacrylate (PEGDMA, M_n=550, Merck), poly (ethylene glycol) methyl ether methacrylate (PEGMEM, M_n=500, Merck), 2,2′-azobis(2-methylpropionitrile) (AIBN, Merck), and lithium sulfonyl(trifluoromethane sulfonyl)imide methacrylate (MTFSILi, Specific Polymers) were used in the experiments. A commercial Li-ion electrolyte made of 1 M $LiPF_6$ in a 50:50 vol. mixture of ethylene carbonate (EC) and dimethyl carbonate (DMC, Merck) was also used.

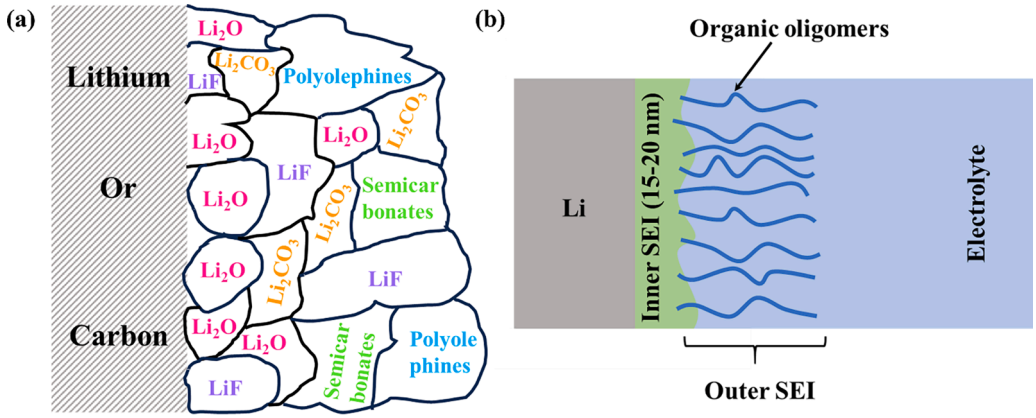

Fig. 1. (a) Early representation of an SEI. Redrawn from [32]. (b) Bi-layered structure of the SEI. Redrawn from [33].

2.2. Preparation of Li foil coated with artificial SEI layer

The coated Li electrodes were fabricated in a Mbraun glove box (Ar atmosphere, O_2 content $\leq$ 0.1 ppm, H_2O content $\leq$ 0.1 ppm) using the dip coating technique in ca. 3 mL PC solutions of 5 wt.% PMTFSILi, 5 wt.% PSTFSILi as well as a 5 wt.% and 10 wt.% of the 1:1 (wt.:wt.) mixture of the two polymers (or only PC). First, the Li foil (50 μm thickness) was punched into round disks with diameters of 12 mm and 15 mm. Then, Li disks were dipped in the PC solutions for 5 min and then dried at room temperature under a dynamic vacuum (10^{-3} bar) for 12 h.

2.3. Cells assembly and measurements

The electrochemical performance of coated Li electrodes was characterized in 2032 coin cells. Li||Li coin cells using a 15 mm and a 12 mm Li disks and a Whatmann GF-A glass fiber mat sandwiched between two Celgard™ H2010 separators were assembled. Plating was done onto the larger electrode for lithium deposits and starting by the larger electrode for cycling experiments. The liquid electrolyte was composed of 1.0 m (mol kg^{-1}) LiFSI in DME. The SISPE was prepared via a facile thermally initiated radical polymerization. PEGMEM (0.7 g 0.0014 mol), PEGDMA (0.077 g 0.00014 mol), MTFSILi (0.2391 g, 0.00069 mol) with initiator AIBN (0.0156 g, 2 wt.% of polymer weight) were added in a vial and kept in the fridge until all the solid powder was dissolved. Then the liquid was cast onto a mold made by two pieces of Mylar foil with a thickness of 200 μm. The polymer electrolyte membrane was formed after heating at 70 °C overnight. The separators of solid-state polymer batteries were prepared by cutting disks in the obtained membrane with a puncher of 19 mm diameter. The cathode slurries were prepared by mixing LFP/ NMC811, PVDF binder, and Super C65 in a weight ratio of 8:1:1 using NMP as the solvent. The LFP and NMC electrodes were made by casting the slurry onto an Al current collector and were punched into 12 mm round disks after drying them in a vacuum oven for 12 h at 80 °C. The mass loadings of LFP and NMC were around 2.8 mg cm^{-2} (or ca. 5.6 mg cm^{-2} when specified in the text) and 2.0 mg cm^{-2} respectively. Before use in lithium metal solid-state batteries, the obtained porous LFP electrodes were infiltrated by 30 μL of the same polymer precursor solution that was used for preparing the single-ion conducting polymer membrane under dynamic vacuum for 30 mins to help wet the LFP electrode. Then, the precursor was polymerized by heating at 70°C for 12 h. Coin cells were cycled with a Neware BTS4000 battery cycler. For LFP||Li cells, within 2.5–3.8 V (1C = 170 mA g^{-1}~ 0.48 mA cm^{-2}) in a Neware temperature-controlled chamber at 25°C and 80°C for liquid-based and solid polymer electrolyte batteries, respectively. NMC811||Li cells were cycled at 25°C within 2.8–4.3 V (1C = 170 mA g^{-1}~ 0.48 mA cm^{-2}) The electrochemical impedance spectra (EIS) were acquired on a VMP2 multichannel potentiostat (Biologic) within the frequency range of 100 kHz ~ 0.01 Hz and an amplitude of 5 mV, excepted for the ionic conductivity and transference number measurements of SISPE when the frequency range of 7 MHz ~ 0.01 Hz and an amplitude of 10 mV was used.

2.4. Materials imaging and characterization

SEM images were obtained using a Zeiss LEO 1550 microscope. The photos were taken with an iPhone 12 (Apple). The cross-section SEM and EDX mapping images of the lithium-metal anode were obtained on a ZEISS Crossbeam XB340, equipped with an energy dispersive X-ray (EDX) spectrometer (Ultim Extreme™, Oxford instruments). The cross-sectional samples were prepared with a Capella FIB with a gallium ion source under a milling current of 1.5 nA. All samples were transferred to the microscope under Argon atmosphere using an air-tight transfer box (SEMILAB) to avoid contamination of the air. The SEM and EDX mapping images were acquired from cross-sectional configuration after FIB preparation using the SmartSEM software for tilt correction to compensate for the image distortion due to the 54° tilt from the optical axis.

X-ray photoelectron spectroscopy (XPS) measurements were carried out in a SPECS UHV system with monochromatic Al Kα radiation (300 W, 15 kV) and a PHOIBOS 150 energy analyzer. To avoid surface contamination, the samples were transferred without air contact from the glove box to the XPS system. The spectra were collected at a take-off angle of 45° and with pass energy of 30 eV at the analyzer for the detail scans. For binding energy calibration of the spectra, the C1s peak of hydrocarbon species (C=C/C-C/C-H) was set to 284.8 eV. The peak fitting of the data was carried out with CasaXPS, using Shirley-type backgrounds and Gaussian-Lorentzian peak shapes (70% Gaussian and 30% Lorentzian, GL30). For the peak fit in the S 2p region, peak doublets with the well-known intensity ratio (2:1) and spin-orbit splitting (Δ = 1.18 eV) were used.

2.5. Electrochemical measurements of the polymer electrolyte

Symmetric coin cells employing stainless steel electrodes (SS|SISPE|SS) were used to test the ionic conductivity via EIS measurements from 30 °C to 100 °C with an interval of 10 °C. The diameter and thickness of the polymer electrolyte were tested with a Mitutoyo micrometer before and after the measurement. Eq. (1) was used to calculate the ionic conductivity (σ) of SISPE:

$$\sigma = \frac{l}{RA} \tag{1}$$

Where l, R, and A are the thickness, resistance, and area of the SISPE used in the coin cells.

Li|SISPE|Li coin cells were used for the determination of the Li-ion transference number at 80 °C via EIS combined with chronoamperometry and calculated by Eqs. (2) and (3).

$$I_0 = \frac{\Delta V}{R_{el,0} + R_{f,0}} \tag{2}$$

$$t_{Li+} = \frac{I_s\left(\Delta V - I_0 R_{f,0}\right)}{I_0\left(\Delta V - I_s R_{f,s}\right)} \tag{3}$$

Where ΔV is the applied voltage of 10 mV, $R_{el,0}$ and $R_{f,0}$ are the initial electrolyte and interfacial resistance, I_s is the steady-state current, $R_{f,s}$ is the interfacial resistance after the chronoamperometry test.

3. Results and discussion

3.1. Preparation of Li foil coated with art-SEI

Many single-ion polymer electrolytes have been reported. Usually, those comprising the most dissociated salt moieties result in polymers that are soluble in a variety of solvents, including those with relatively low dielectric constants such as DMC and dimethoxyethane (DME), unless they are crosslinked, either chemically or physically, in which case they can still be swollen by solvents. It is the case, for instance, of an imide anionic moiety perfluorinated on both sides, which is favorable for ionic conductivity as the absorbed plasticizer enhances ion transport, but would be detrimental for blocking electrolyte species [3,34]. Also, based on the bis(trifluoromethanesulfonyl)imide anion ($TFSI^-$), several pending moieties can be found that result in various degrees of dissociation and miscibility with ether solvents. Bouchet et al. [35] and Porcarelli et al. [36]. used a pending imide anion that resembles the TFSI anion on one side but does not include a perfluorinated chain on the other side, attached to either a polystyrene or polymethacrylate backbone, respectively. As a result, the polystyrene homopolymer, is immiscible in low dielectric constant solvents such as DMC, DME or is immiscible with polyethylene oxide blocks, allowing the preparation of a phase separated block copolymer system. Thus, single-ion homopolymers based on the same repeating anionic moiety and with either a

polystyrene or a polymethacrylate backbone were used here, i.e., PSTFSILi and PMTFSILi as represented in Fig. 2a-b, to make use of their different solubility in ether solvents.

PMTFSILi, PSTFSILi, as well as their mixture (1:1 in weight ratio) were dissolved in propylene carbonate (PC) to form solutions with 5 wt. % polymer. These solutions were used to form the art-SEIs on Li foils via dip coating for further tests in ether-based electrolytes. The obtained lithium anodes coated with PSTFSILi, PMTFSILi, and their mixture are named as *PS, PM*, and *PS+PM*, respectively. The coating obtained was rather thin with a mass loading of 0.11 mg cm^{-2} (± 25 %), so an estimated thickness of ca. 1.0 μm ± 0.4 (estimating the density between 1 and 1.5 g cm^{-3}). In addition, as references, pristine anodes (noted *bare*) were used, as well as anodes dipped in pure PC following the same protocol (noted *PC-only*) to differentiate the effect of PC, a priori reduced into a carbonate-rich layer during processing and the effect of the polymer coating.

The affinity of the polymer 1:1 mixture with DME was examined via the preparation of membranes. After dissolving the two polymers in PC, it is possible to obtain membranes (via solvent casting) that seem homogeneous, although rather brittle (Fig. 2c). They can be gelled by dipping them in DME as illustrated in Fig. 2d, to obtain a rather soft gel, as shown in Fig. 2e. Since PSTFSILi is not soluble in DME and PMTFSILi is, it is likely that the PMTFSILi fraction of the membrane is swollen by DME and that the PSTFSILi fraction allows keeping dimensional stability. Fig. 2f and g show the appearance of the *bare* Li disk and the *PS+PM* coated disk. After coating, the surface of lithium seems smoother and shinier, although some surface features can still be seen through the coating.

3.2. Art-SEIs performance in a liquid electrolyte

In a first step, the Li metal anodes were tested in symmetrical Li|electrolyte|Li cells using an ether-based liquid electrolyte made of 1 m (mol kg^{-1} of solvent) lithium bis(fluorosulfonyl)imide (LiFSI) in DME. The voltage profiles of the cells upon polarization at various current densities are shown in Fig. 3a-c. In all cases, the voltage shows a steep jump followed by a voltage relaxation reaching a plateau upon time. However, at 0.1 mA cm^{-2}, a rapid decline of voltage to ca. 0.01 V occurs for the cells with the *bare* and *PC-only* Li disks. This can be attributed to the uneven deposition and significant dendrite growth leading to increased surface area of Li metal and consequently a decrease in resistance. In comparison, the voltages of Li||Li cells with *PS, PM* and *PS+PM* art-SEIs stabilize at a relatively higher value after experiencing only a slight initial drop, indicating that the surface area and overall SEI resistance are better preserved.

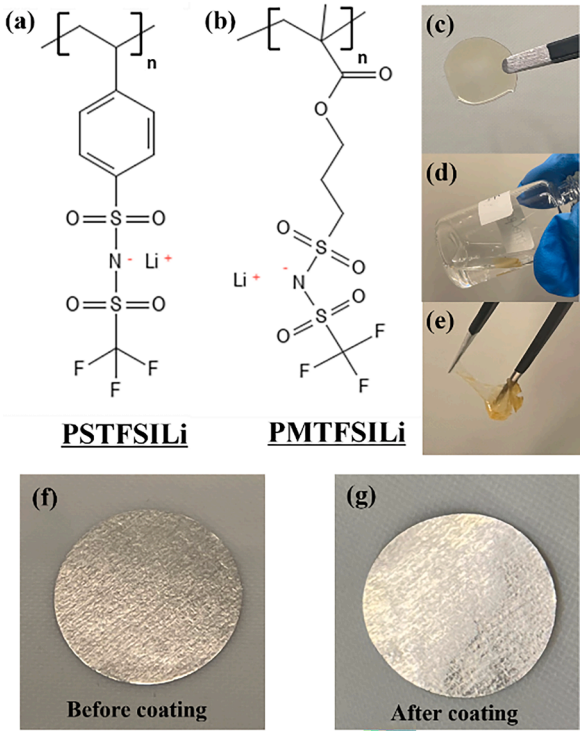

Fig. 2. Molecular formulae of the single-ion polymers used in this study (a) PSTFSILi, (b) PMTFSILi. The appearance of a membrane obtained by (c) casting a 2.5 wt.% PSTFSILi + 2.5 wt.% PMTFSILi/PC solution and drying at 70 °C in a glove box. (e) the gel obtained after dipping the dry membrane in DME, as shown in (d). *Bare* (f) and *PS+PM* (g) coated lithium disks.

This is confirmed by EIS results shown in Fig. 3d-e. The cells using *bare* Li electrodes exhibit a significant reduction of the interfacial resistance due to dendrite growth. In stark contrast, cells employing *PS+PM* electrodes exhibit an increased resistance after plating (Fig. 3e). The results obtained with *PC-only* art-SEI are like those of *bare* Li disk (Fig. S1a), whereas the cells using single polymer coatings also show a resistance increase after plating (see Fig. S1b-c). Although the increase of SEI resistance is not suitable a priori, its decrease via the increase of lithium ('fresh') surface area is detrimental to long-term performance since, over cycling, the initial decrease is usually followed by an increase, as 'fresh' lithium is replaced by a layer of lithium and electrolyte degradation products that ultimately limits lithium transport. On the other hand, the slight increases observed with the coated electrodes are expected as the SEIs thickness or resistivity evolve in contact with the electrolyte via the formation of electrolyte reduction products, unless other phenomena such as SEI stretching, cracking or increase of electrode surface area occur (e.g. as a result of dendrite growth).

At higher current densities of 0.25 mA cm^{-2} and 0.5 mA cm^{-2}, the voltage difference between cells employing the different art-SEIs are more pronounced. Indeed, only the art-SEI formed from the *PS+PM* solution leads to a relatively constant plating voltage (Fig. 3b-c).

To visualize the influence of the art-SEIs on the homogeneity of Li metal plating, the cells employing *bare, PC-only, PM, PS*, and *PS+PM* electrodes were dismantled and subjected to visual observation. As shown in Fig. 4a and Fig. S2a, after Li plating at a low current density of 0.1 mA cm^{-2} for only 5 h, the *bare* and *PC-only* Li disks, respectively, exhibit obvious protrusions on their surfaces and dendrites have grown into the separators. In contrast, even after plating at the same current density but for 20 h, the electrodes coated with *PM, PS*, and *PS+PM* remain shiny and no obvious dendrite growth can be seen on the separators (Fig. 4b and Fig. S2b-c, respectively).

The SEM images of the bare Li electrode after 5 h plating at 0.1 mA cm-2 (Fig. 4c) show small protrusions covering most of the surface of the electrode and the presence of aggregated protrusions (seen also in Fig. 4e), confirming the inhomogeneity of the deposit. The SEM images of the *PC-only* treated electrodes after 5 h plating at 0.1 mA cm^{-2} also show areas with protrusions (Fig. S3a), and some of them appear to have a rod-like shape with sub-micrometric dimensions (Fig. S3b). These images with smaller dendrites are coherent with the observed growth into the separator presented previously. By contrast, the surface of the *PS+PM* electrode after 20 h plating at 0.1 mA cm^{-2} (Fig. 4d) exhibits no protrusions in most areas (see also Fig. S3c for a zoom on an area without protrusions), although some aggregated protrusions can still be observed in some places. Nevertheless, zooming onto one of these areas (Fig. 4f) indicates that the plating remains rather dense and flat, in accordance with the lack of dendrite growth into the separator. Similar-looking SEM images are shown in Fig. S3d-f for the *PM* treated anode after 20 h of plating at 0.1 mA cm^{-2}.

For the *PS* electrode, it was even possible to plate Li for 92.5 h at 0.1 mA cm^{-2} before reaching the cut-off voltage of 3 V. In this case, the surface of the anode is not flat anymore (Fig. 5a). However, no black dendrite growth could be observed on the separator (Fig. 5b), although almost all the lithium of the stripped electrode has been transferred onto the plated electrode (Fig. 5c). A closer look at the plated anode reveals

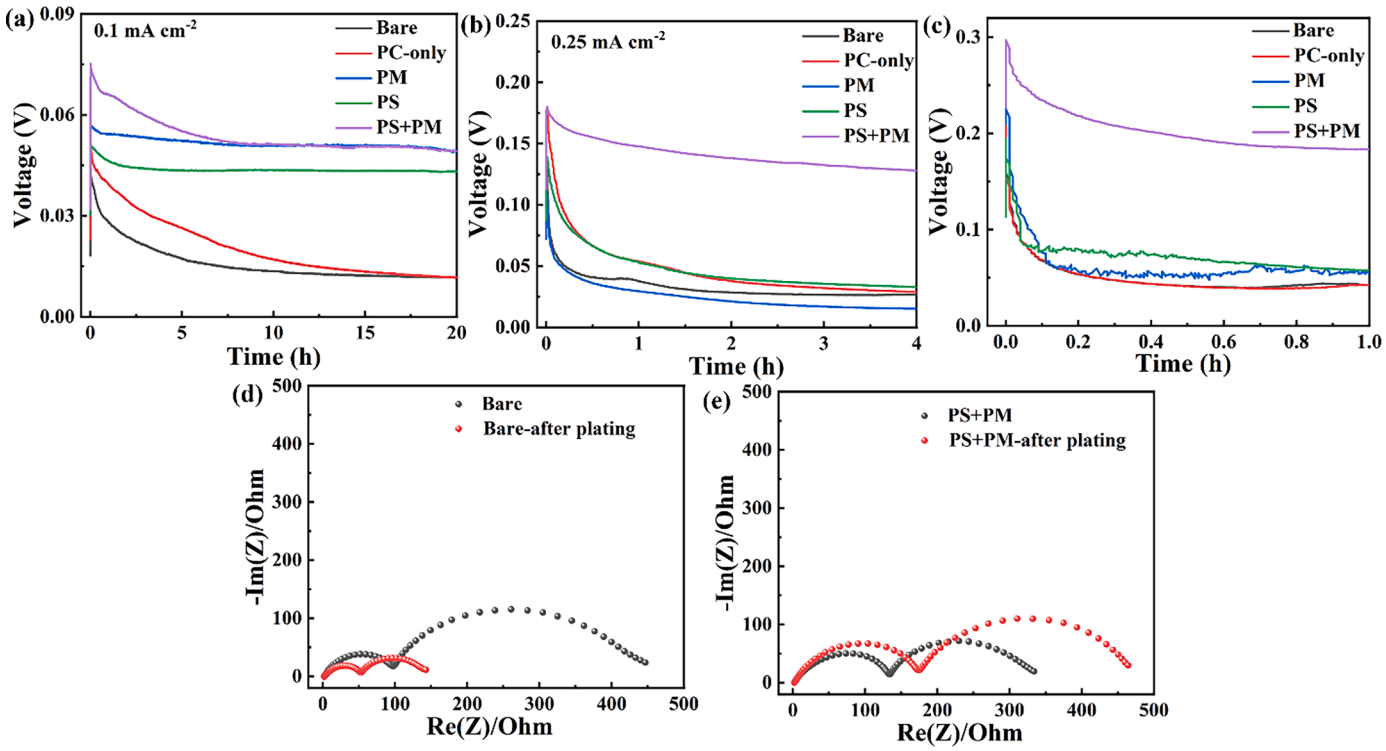

Fig. 3. Voltage profiles of Li||Li cells using different Li metal anodes with different current densities: (a) 0.1 mA cm^{-2}, (b) 0.25 mA cm^{-2}, and (c) 0.5 mA cm^{-2}. Impedance spectra of the cells before and after galvanostatic experiments for 20 h at 0.1 mA cm^{-2}. (d) *Bare* Li; (e) *PS+PM* Li electrode.

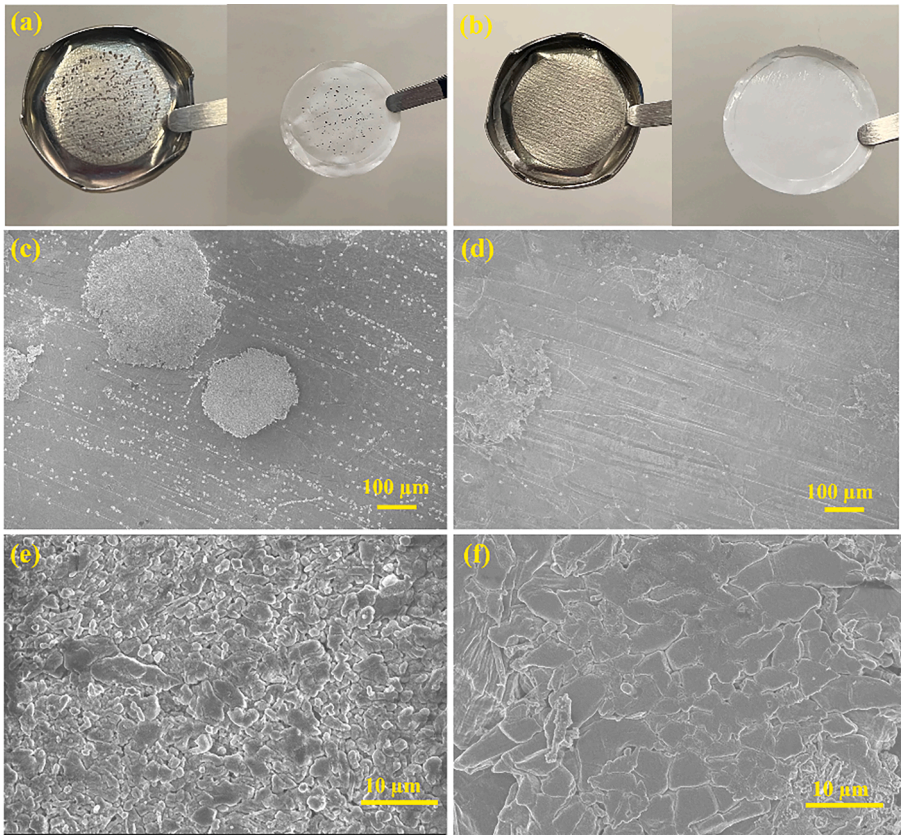

Fig. 4. Images of Li electrodes and separator (a) after plating at 0.1 mA cm^{-2} for 5 h using *bare* Li electrode and (b) after plating at 0.1 mA cm^{-2} for 20 h using a *PS+PM* Li electrode. Corresponding SEM images of (c,e) *bare* electrode (d,f) *PS+PM* electrode.

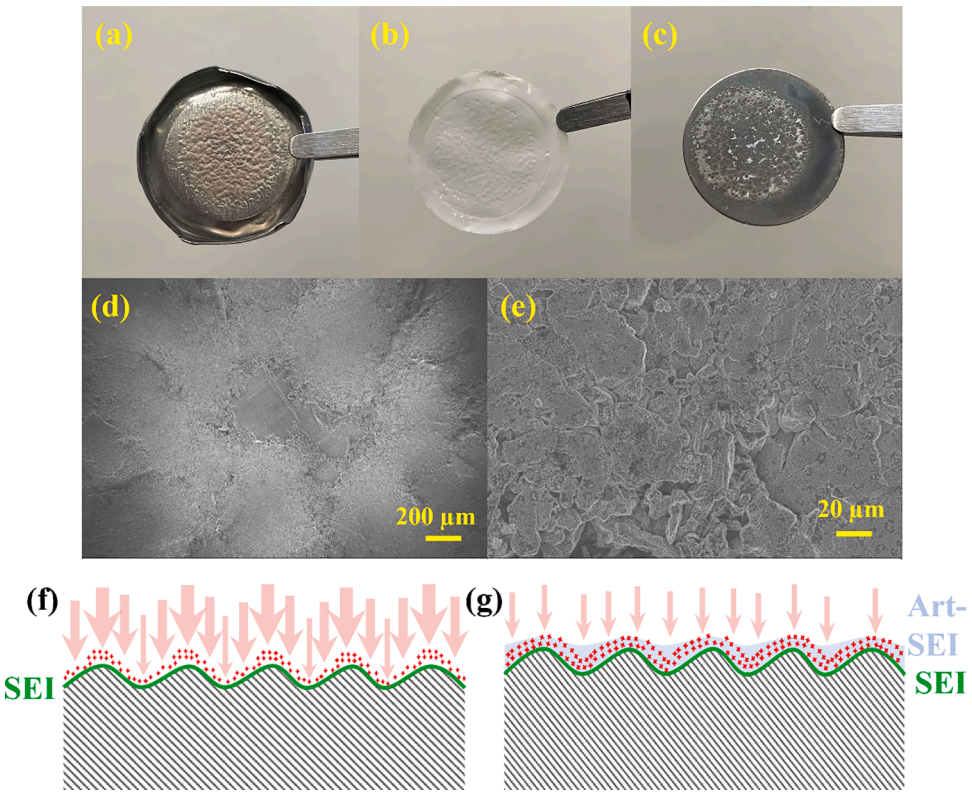

Fig. 5. Photos of (a) plated Li electrode, (b) separator, and (c) stripped Li electrode unmounted from a Li||Li cell employing *PS* Li electrodes after Li plating at 0.1 mA cm^{-2} for 92.5 h. (d,e) SEM images of the plated *PS* electrode shown in (a). Schematic illustration of Li deposition on the surface of (f) *bare* Li and (g) art-SEI coated Li disks.

that most of the surface is covered by protrusions, but these are, in this case as well, rather flat and dense (Fig. 5d-e), confirming the excellent protection against dendrite growth of the *PS* art-SEI at this current rate.

At the higher current density of 0.25 and 0.5 mA cm^{-2}, the photographs of plated Li electrodes and corresponding separators confirm that the *PS*+*PM* art-SEI outperforms the *PS* and *PM* electrodes, as for the former two electrodes, black dendrites have grown into the separator after Li deposition (Fig. S4 and S5). This indicates that the combination of the two polymers is more favorable for practical use at higher current densities.

The differences in behaviors of the art-SEI can be explained as follow: Although all the art-SEIs allow improvements vs. uncoated electrode, the *PS* art-SEI is a priori the more robust since it does not absorb DME, thus it allows excellent protection, but at the cost of a low conductivity, due to the lack of solvating functions.

Therefore, it leads to excellent performance at low current at which its conductivity is still sufficient. On the other hand, we can see that the *PS*+*PM* art-SEI is far superior when using higher current, vs. both the *PM* and PS art-SEI. It is likely that the polymer mixture gives, in this case, the best compromise between robustness vs. solvent ingress and conductivity. For all art-SEI, the effect of having a constant lithium concentration at the lithium/electrolyte interface (or more constant, depending on electrolyte uptake) is illustrated in Fig. 5f-g. Fig. 5f shows that, with *bare* Li, the surface roughness (observed on Fig. 2f) results in inhomogeneous concentration of Li^+ at the Li/electrolyte interface and thus inhomogeneous current density that favors increased inhomogeneous deposition (as for any protrusion). Having a constant concentration at the interface thanks to a single-ion conducting art-SEI limits irregularities of concentration and current densities (providing that the current density is homogenous in the electrolyte), as illustrated in Fig. 5g.

3.3. Effect on long-term cycling

The *PS*+*PM* and *bare* Li anodes were selected for long-term cycling tests of Li||Li symmetrical cells. The voltage profiles of the cells cycling at 0.1 mA cm^{-2} with a capacity of 0.1 mAh cm^{-2} or 1 mAh cm^{-2} are shown in Fig. 6a and b, respectively. As shown in the inserts, the cells using *PS*+*PM* Li disks exhibit a more stable voltage in the early cycles, indicating that the single-ion conducting art-SEI helps achieve more homogeneous plating and stripping. As can be seen, when cycling at 0.1 mAh cm^{-2}, the cell with the art-SEI cycles more steadily with a less erratic variation of voltage, compared with the *bare* Li cells. Also, the *bare* cell cycled at 0.1 mA cm^{-2} exhibits a voltage surge up to 3 V after 582 h, which corresponds to the full lithium consumption of one electrode. Besides, prior to the voltage surge, a continuous increase of voltage is observed, as over cycling, electrolyte is consumed, and unfavorable degradation products layers are formed. For the modified symmetric cell, however, a voltage hysteresis below 0.1 V is maintained for more than 1200 h, which confirms that the art-SEI is beneficial to improve long-term cycling stability. A similar improvement is obtained when cycling a larger Li capacity of 1 mAh cm^{-2}, although in this case, the *PS*+*PM* cell fails shortly after 660 h.

To improve the results further, a thicker art-SEI layer was prepared using 5 wt.% PMTFSILi + 5 wt.% PSTFSILi PC soluition (noted as *5 wt.% PS+5 wt.% PM*) with the same protocol. The mass loading of the thicker coating layer was 0.40 mg cm^{-2} (± 25 %) with an estimated thickness of ca. 3.5 μm ± 1.5 (estimating the density between 1 and 1.5 g cm^{-3}). As shown in the insert of Fig. S6, the thicker art-SEI helps maintain a stable voltage for longer periods, up to 80 h at 0.1 mAh cm^{-2} and 100 h at 1 mAh cm^{-2}. These values are 30 h and 40 h respectively with the thinner *PS*+*PM* art-SEI. Noticeably, with the thicker art-SEI, the long-term cycling performance is significantly enhanced up to 1100 h when cycling 1 mAh cm^{-2} (Fig. S6b) before the voltage surge appears.

To characterize the evolution of the interlayer during cycling,

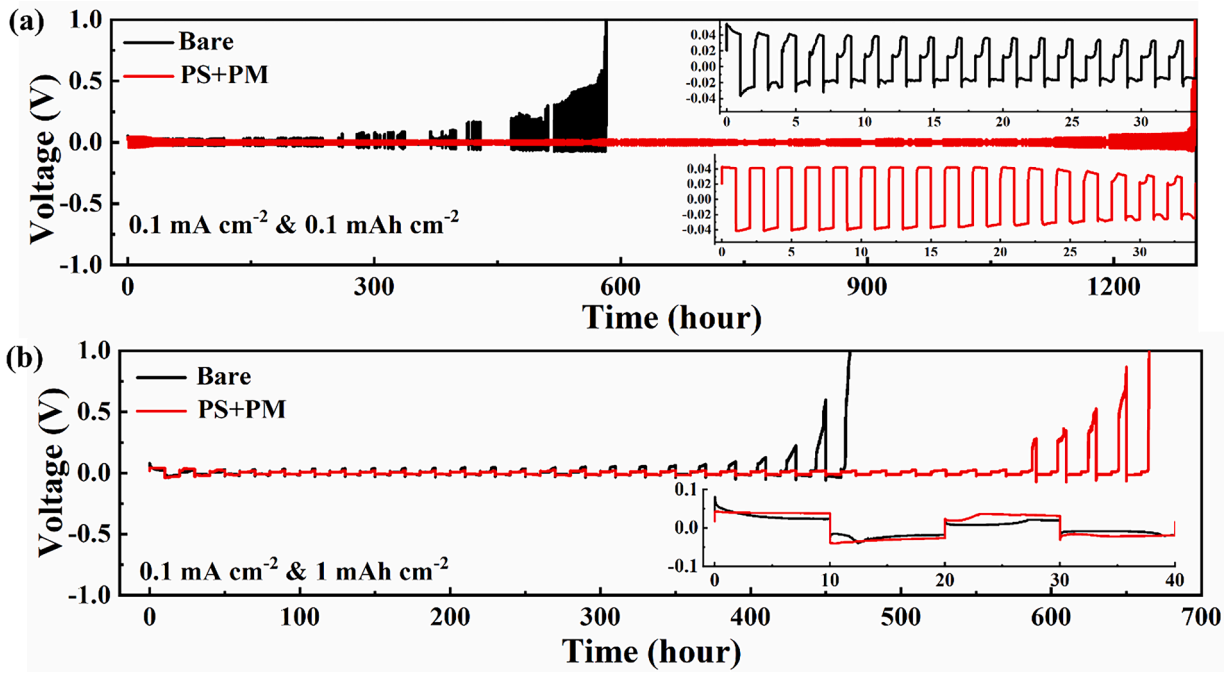

Fig. 6. Voltage profiles of Li symmetric cells using 1 m LiFSI in DME electrolyte at 0.1 mA cm^{-2} with a cycling capacity of (a) 0.1 mAh cm^{-2} and (b) 1 mAh cm^{-2} for each plating/stripping step.

impedance measurements of cells using *bare* Li and *PS+PM* Li cells were carried out periodically during cycling at 0.1 mA cm^{-2} (1 h steps), and the corresponding Nyquist plots are shown in Fig. S7. All spectra exhibit two semi-circles. For *bare* Li cells, the resistances associated with each semi-circle significantly decreases over cycling, indicating an increased area of the interface due to dendrite growth. In contrast, for coated Li cells, the resistance corresponding to the first semi-circle, usually considered to be related to the SEI, increases after the first cycle, and then stays relatively stable in the subsequent cycles and the resistance corresponding to the second semi-circle only slightly decreases over cycling. This is a further indication that the coated layer help stabilize the interface and limit the dendrite growth.

Besides, the cycling performance of *bare* Li and *PS+PM* Li cells was tested using a classical alkyl carbonate electrolyte (1 M $LiPF_6$ in EC/DMC= 50/50). As shown in Fig. S8, when cycling at 0.5 mA cm^{-2} a capacity of 0.1 mAh cm^{-2}, the overvoltage of *bare* Li cells significantly decreases from 0.35 V to 0.11 V during the first 10 h, while the *PS+PM* Li maintains a relatively stable overvoltage during the first 50 h. Also, a voltage surge up to 1.5 V occurs at around 197 h for the *bare* Li cells and 248 h for *PS+PM* Li cells respectively. The improvement in terms of cycling stability is more limited in this case probably as the unreacted part of the coated layer can quickly dissolve in PC.

The performance of *bare* and *5 wt.% PS+5 wt.% PM* Li anodes has been further tested in LFP ||Li cells. As shown in Fig. S9, the *5 wt.% PS+5 wt.% PM* cell exhibits a significantly improved capacity retention of 91 % with 150.4 mAh g^{-1} in the 100th cycle at 0.5C, which is higher than the 83 % of the *bare* cell (132.9 mAh g^{-1}). A similar improvement can also be found when using a higher mass loading of LFP (5.6 mg cm^{-2}) and a lower C-rate (0.2C) as shown in Fig. S10, with a 97 % capacity retention after 100 cycles (vs. 90 % for the uncoated cell), which confirms the effectiveness of the art-SEI.

Although the use of classical carbonate-based electrolytes such as 1 M $LiPF_6$ in EC/DMC (1:1, vol.) is likely to induce some dissolution of the coatings, some NMC811||Li cells were assembled and tested using *5 wt.% PS+5 wt.% PM* Li electrodes and the cycling results are shown in Fig. S11. In this case, the coating also helps improve the cycling stability of the cells with a capacity retention of 71 % after 100 cycles for the cell with coated Li and 52 % for the cell using a bare Li anode.

3.4. Surface analysis of the art-SEI

The chemical state and elemental composition in the surface layers of the coated lithium disks were characterized by XPS and the results are displayed in Fig. 7 that shows the detailed spectra in the C1s, O1s, and F1s regions and Fig. S12 (for the Li1s, S2p, and N1s regions). The elemental compositions are compiled in Table 1 and the percentages of the various species from the peak fittings are tabulated in Tables S1-S7 for all detected elements. The measurements were carried out on lithium anodes coated with PSTFSILi, PMTFSILi, 2.5 wt.%+2,5 wt.% PMTFSILi (noted as *PS layer, PM layer* and *PS+PM layer* respectively), and on PS+PM layer samples which were in contact with electrolyte for 24 h (without cycling) or subjected to 20 cycles in a Li||Li cell (0.1 mA cm^{-1}, 1 h step duration), noted as *PS+PM SEI 24 h* and *PS+PM SEI 20 cycles* respectively.

The detail spectra in the C1s region (Fig. 7a, Table S1) show, for all samples, a dominating peak at 284.8 eV due to C=C/C-C/C-H (hydrocarbon) species [37]. At higher binding energy follow features due to C-O (286.3 eV), C=O (288.5 eV), and O-C=O (carboxyl/carbonate) (289.8 eV) moieties that are, for the PS layer, most probably resulting from PC decomposition during the formation of the coating layer although for the PM layer, ester groups decomposition products also contribute. Finally, the CF_x (292.7 eV) peak has a rather low intensity except for the cycled sample. The O1s spectra (Fig. 7b, Table S2) can be fitted with two peaks that correspond to different contributions: the first peak at 531.6 eV is assigned to O=C groups and O-C=O/carbonates and the second feature at 533.2 eV is related to O-C and O=S species (the latter from SO_2CF_3/SO_2F groups) [38–40]. Interestingly, no signal corresponding to Li_2O is observed in the O1s spectra of any of the deposited layers, which shows that the surface of lithium is buried below a layer that is thicker than the XPS sampling depth and well covered by the art-SEI. Two types of F species can be discerned in the F1s detail spectra (Fig. 7c, Table S3): the peak at lower binding energy (685.1 eV) is due to LiF, while C-F/S-F functionalities from SO_2CF_3/SO_2F groups lead to the other peak at higher binding energy (688.5 eV) [39–41]. In brief, the spectra in the Li1s, S2p, and N1s regions (Fig. S12) show for all samples a single Li1s peak at ~55.3 eV (Fig. S12a, Table S4), a dominating peak doublet due to SO_2CF_3/SO_2F groups ($S2p_{3/2}$ peak at ~169 eV) and a

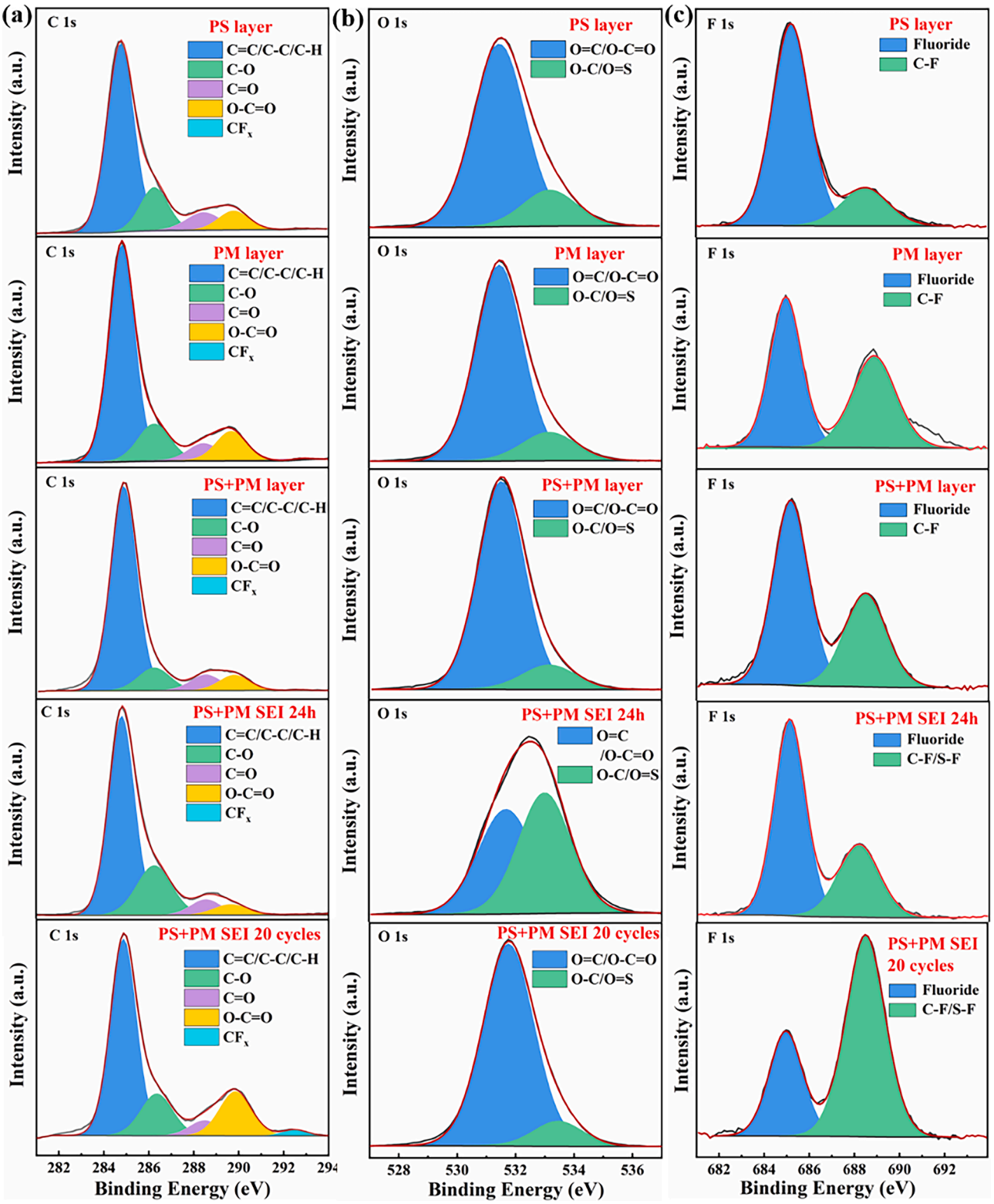

Fig. 7. XPS detail spectra in the (a) C1s, (b) O1s and (c) F1s region for Li anodes coated with PS, PM, or PS+PM layers (without electrolyte contact), a PS+PM SEI layer after 24 h contact with electrolyte, and a PS+PM SEI layer after 20 cycles.

much smaller feature due to its decomposition products (SO_x – $S2p_{3/2}$ peak at ~167 eV) in the S2p detail spectra (Fig. S12b, Table S5), and a single imide N1s peak at ~399.3 eV for all samples and an additional smaller feature at 397.3 eV (nitride) for the cycled sample (Fig. S12c, Table S6) [42,43]. Finally, it should be noted that a small amount of Cl^- impurities was detected in all deposited layers (Table S7), likely originating from the starting polymers.

In terms of elemental compositions, we compare in Table 1 the results derived from XPS measurements to the theoretical compositions of the polymers. Starting with the as-deposited layers, the fraction of carbon is, in all cases, very similar with around 42–43 % and no clear trend based on the polymer compositions can be seen. The lithium content is

Table 1
Results of the quantitative XPS analysis for the different layers deposited onto lithium disks (noted as *layer*), after 24 h electrolyte contact (noted as *SEI 24 h*), and after 20 cycles in a Li||Li cell (0.1 mA cm^{-1}, 1 h steps), noted *SEI 20 cycles*. For comparison, the theoretical compositions of PSTFSILi and PMTFSILi are also given.

Element	PSTFSILi (th.)	PMTFSILi (th.)	PM layer (XPS)	PS layer (XPS)	PS+ PM layer (XPS)	PS+PM SEI 24 h (XPS)	PS+PM SEI 20 cycles (XPS)
C /%	45.00	38.10	42.95	41.95	43.15	37.78	34.24
Li /%	5.00	4.76	18.96	16.57	19.10	15.07	20.81
O /%	20.00	28.57	33.25	31.23	30.81	28.65	35.59
F /%	15.00	14.29	2.92	8.05	4.40	8.00	4.35
S /%	10.00	9.52	0.94	0.96	1.40	7.43	3.27
N /%	5.00	4.76	0.46	0.50	0.64	3.07	1.74
Cl /%	–	–	0.52	0.74	0.49	–	–

much higher than what is expected for the polymers. The lithium excess most probably results from Li-containing products formed by the reaction of the polymers and PC with Li metal during coating. The oxygen fractions, around 30 % for all deposited layers are higher than those of the starting polymers. It can be noted that the *PS* layer has an oxygen content ca. 50 % higher than PSTFSILi, whereas the *PM* layer has approximately the same oxygen content as the starting polymer. This suggests that the PM layer contains more PMTFSILi reduction products than PC reduction products, as compared with the PS layer (i.e. a higher reactivity of PMTFSILi vs. PSTFSILi). This is not surprising since the ester groups in PMTFSILi are easily reduced. In contrast, the F, S, and N contents are in all cases much smaller than expected. For F, significantly different concentrations are observed in the PM (2.92 %), PM+PS (4.40 %) and PS (8.05 %) layer. Interestingly, the peak fitting (Fig. 7c, see also Table S3) demonstrates that these differences are mainly related to LiF content, while the C-F contribution is comparable for all three samples (~1.5 %). The concentrations of N and S are relatively similar for the PS and PM layers. In contrast, the PS+PM layer contains slightly more S and N elements. Thus, although the composition of the PM+PS layer seems to fall in between those of PS and PM layers in terms of LiF content, the higher sulfur and nitrogen content confirms that the PM+PS layer contains more of the polymers and their degradation products rather than those from the reduction of PC during the layer deposition. In the case of the PS layer, since the polystyrene backbone is less reactive, more PC and anionic functions react, leading to more LiF and O-containing degradation products (C-O, C=O, and O-C=O). For the PM layer, less LiF is formed while it has the highest O-C=O content (due to the carboxyl group in PMTFSILi). Taken together, the mixture of the polymers leads to a layer with an intermediate LiF content, the lowest O-C=O (carbonate) content, and the highest nitrogen and sulfur content. This indicates that the PS+PM polymer mixture reduce the formation of PC decomposition products during the coating step, compared to PS, due to the reactivity of the polyester backbone, that also limits the reduction of anionic functions. Thus, beyond the expected differences in terms of electrolyte uptake, it seems that, even prior to being in contact with the electrolyte, the layers differ significantly in terms of the proportion of polymer backbone, anion, and PC degradation products.

Since the PS+PM art-SEI led to the best plating and cycling results, it was investigated further by XPS to get insight into the surface evolution upon contact with the 1 m LiFSI in DME electrolyte. The results of the quantitative analysis for this sample, in Table 1, show that the amounts of C, O and Li decrease slightly whereas the fractions of F, S and N increase. This was expected since LiFSI and DME penetrate upon contact into the layer and react, which can be seen for example by the doubling of the (ether) C—O species contribution (from 4.50 % to 8.47%) in the C1s spectra (Fig. 7a), likely resulting from DME reduction. Furthermore, the increase of F, S and N concentration results from the presence of LiFSI and/or its decomposition products. As an example, the F1s spectrum (Fig. 7c) shows both an increase of the LiF and C-F/S-F signal compared to the PS+PM layer (from additional LiFSI) and the same trend is also observed in the S2p and N1s regions. Overall, the oxygen content decreases slightly, although all compounds (LiFSI and DME) have higher O content than the deposited layer. This could be due to a rearrangement of the layer upon swelling and drying. In terms of functional groups, as shown by the O1s spectra in Fig. 7b, the layer exhibits a higher fraction of C-O and S=O groups, which corroborates the results seen in the C1s and S2p regions. The Li content decreases, in agreement with the presence of unreacted LiFSI salt (as its Li content is lower than that of the deposited layer) and the Cl^- impurities disappear.

During cycling, the layer evolves further, with a decrease of the carbon content, an increase in Li and O and a decrease in S, N and F (Table 1). Interestingly, the O1s spectrum (Fig. 7b) still does not exhibit any feature related to Li_2O (expected at ~528.5 eV). This seems to indicate that the layer is still well covering the lithium surface. Furthermore, the spectrum (Fig. 7b, Table S2) shows an increase of the O=C/O-C=O signal and a doubling of the concentration of the related species. This goes along with a significant increase of the O-C=O (carbonate) peak in the C1s spectrum (Fig. 7a).

To assess the thickness and elemental composition of the art-SEI, cross-sectional SEM and corresponding EDX images of *PS+PM* Li were acquired after coating and after 20 cycles. As shown in Fig. S13, a layer of ca. 0.85 µm thickness is clearly seen after coating. EDX images for O, C, F, and S elements confirm that the layer 'as deposited' covers uniformly the surface of the Li anode. As shown in Fig. 8, after 20 cycles at 0.1 mA cm^{-2} (1 h per step), a dense and smooth interlayer is maintained without any evidence of dendrite growth.

3.5. Combination of art-SEI and SISPE

Even though improvements linked to the coating of single-ion art-SEI onto lithium are clearly observed, using a liquid electrolyte paired with a separator did not enable very long-term cycling of lithium. This was expected, since microporous separators such as Celgard do not enable

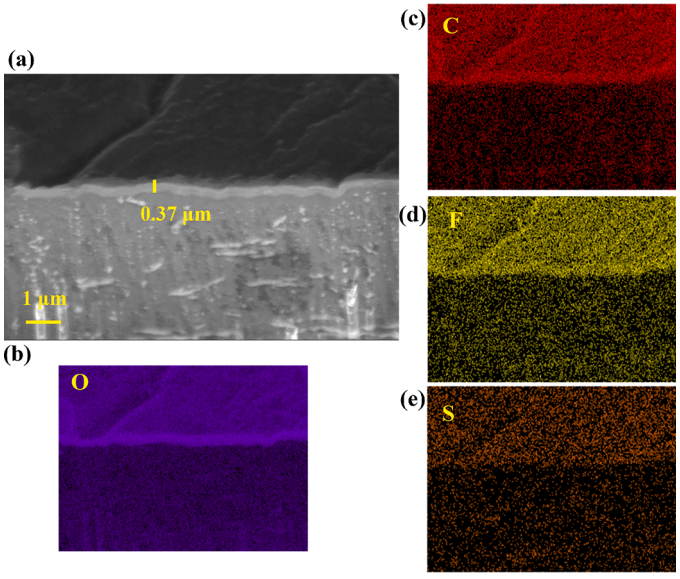

Fig. 8. (a) Cross-sectional SEM image of *PS+PM* Li after 20 cycles of stripping/plating, and corresponding EDX images of (b) O, (c) C, (d) F, (e) S elements.

homogeneous pressure onto the lithium electrode, which leads to the growth of lithium in the 1D pores of the Celgard separators. Besides, it can also induce inhomogeneity of current density and/or Li surface damage. Although the art-SEI can, in principle, help homogenizing the pressure and current density, polymer electrolytes are more suitable for these duties being themselves homogeneous at the molecular level. As electrolytes have thicknesses well above art-SEI, it is crucial to enable a relatively high conductivity by adding PEO domains that solvate Li^+ and help increase ionic mobility. Thus, a crosslinked single-ion comb polymer with a methacrylate backbone was prepared as a polymer membrane, using poly(ethylene glycol) methyl ether methacrylate (PEGMEM) as monomer, poly(ethylene glycol) dimethacrylate (PEGDMA) as a crosslinker, and lithium sulfonyl(trifluoromethanesulfonyl)imide methacrylate MTFSILi (see Fig. 9a-d for the molecular formulae of the reagents) as monomeric Li salt to form a SISPE with a PEGDMA:PEGMEM molar (crosslinker) ratio of 1:10 and an O/Li ratio of 20 (O corresponding the ether oxygen onto the PEO chains). After the thermal radical polymerization, transparent polymer membranes were obtained (See Fig. 9e).

The transference number of the polymer electrolyte was measured as 1 ± 0.05 (more details shown in Fig. S14), using the 'Bruce and Vincent' method [44] modified by Watanabe et al. [45] and the conductivity at 80 °C is 5.8×10^{-6} S cm^{-1} (further details in Fig. S15).

The polymer electrolyte was then used to assemble Li||Li symmetric cells with either *bare* or *PS+PM* lithium electrodes. As shown in Fig. 9f, the overvoltage of the cell using coated art-SEI is barely affected by cycling for over 5000 h (without failing) while that of the cell using *bare* Li disk gradually increases and ends up above 1.5 V after ca. 2000 h, indicating that coated Li disks possess a more stable interface. In this case, since both systems have the same SISPE, the differences are not a priori attributable to the single-ion conduction within the art-SEI. Most likely the mechanical properties of the SEI or the better homogeneity of the current density within the SEI explains the improvements since protrusions non-related to concentration gradient (i.e., 'bottom grown' protrusions) are limited, in addition to the concentration gradient-related 'tip grown' dendrites that are limited in both cases by use of single-ion electrolyte.

To demonstrate the possibility to cycle LFP||Li solid-state polymer electrolyte batteries, porous Li-ion battery LFP electrodes were used to prepare dense lithium metal polymer battery cathodes including the SISPE. To do so, the same polymer precursor mixture used to prepare the SISPE membrane was infiltrated into the LFP pores by applying dynamic vacuum for 30 min with a rotary pump and polymerized at 70 °C for 12 h. The cathodes were then used to assemble lithium metal polymer batteries with either *bare* or *5 wt.% PS+5 wt.% PM* anodes and SISPE membranes. The cycling results are compared in Fig. 9g. As can be seen, the initial capacities of the cells are similar. However, the capacity retentions differ considerably with 80 % of the initial capacity reached at 75 cycles for the *bare* cell vs. 135 cycles for the *5 wt.% PS+5 wt.% PM* Li cell, although both cells exhibit efficiencies close to 100 % after the first cycle.

4. Conclusion

In summary, we have demonstrated single-ion conducting art-SEIs based on polystyrene (PSTFSILi) and/or polymethacrylate (PMTFSILi) anionic functional moiety for improved Li deposition and suppression of dendrite growth. This is confirmed by the visual and SEM observation of plated Li electrodes and corresponding separators. The combination of these two polymers outperforms the single polymer art-SEIs at higher current density of 0.25 and 0.5 mA cm^{-2}, resulting from the synergy of properties, including their different solubilities in ether-based liquid electrolytes. The mixed polymer art-SEI enables better cycling stability in both Li||Li symmetric cells and LFP||Li cells compared with cells using untreated Li. This likely results from improvements in lithium metal confinement and the homogeneity of the current density, as concentration gradients close to the Li metal are limited as well as the direct contact between the Li metal anode and the separator. Finally, the

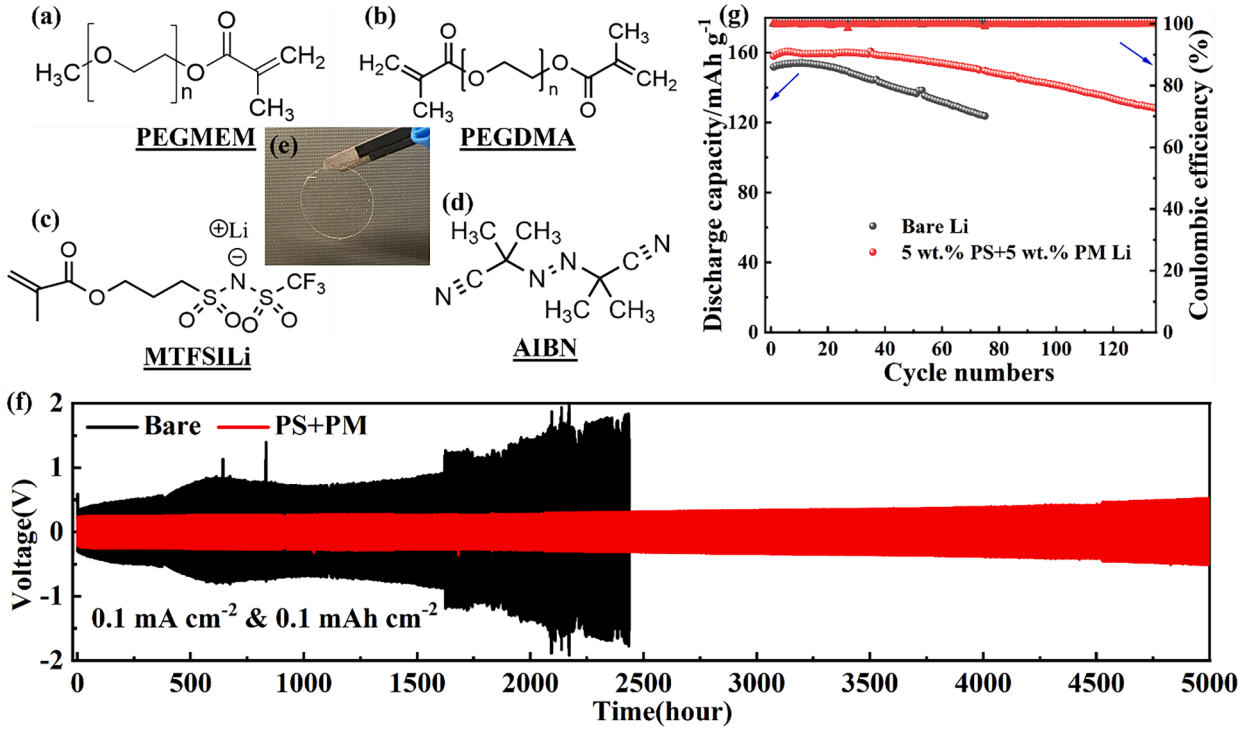

Fig. 9. Molecular formulae of the chemicals used to synthesize the single-ion conducting polymer electrolyte. (a) PEGMEM, (b) PEGDMA (c) MTFSILi (d) AIBN. (e) appearance of the obtained SISPE. (f) long-term cycling of symmetrical Li||Li cells at 80 °C employing single-ion conducting polymer membrane and either coated or *bare* lithium anodes at 0.1 mA cm^{-2} with a capacity of 0.1 mAh cm^{-2}. (g) cycling performance of lithium metal solid-state batteries (LFP|SISPE|Li cells) cycling at 80 °C at 0.2 C.

combined use of SISPE and single-ion conducting art-SEI layer significantly enhances the long-term cycling performance of the Li metal anode and that of lithium metal polymer battery cells.

CRediT authorship contribution statement

Jiajia Wan: Investigation, Conceptualization, Writing – original draft, Data curation. **Xu Liu:** Investigation, Supervision. **Thomas Diemant:** Investigation, Data curation. **Mintao Wan:** Investigation, Data curation. **Stefano Passerini:** Funding acquisition, Supervision, Writing – review & editing. **Elie Paillard:** Conceptualization, Funding acquisition, Supervision, Writing – review & editing.

Declaration of Competing Interest

The authors declare the following financial interests/personal relationships which may be considered as potential competing interests:

Elie Paillard reports financial support was provided by European Commission. Jiajia Wan reports financial support was provided by China Scholarship Council.

Acknowledgement

The research presented here has been supported by the European Commission via Project VIDICAT (GA 829145). J.W. was financially supported by the China Scholarship Council (CSC).

Supplementary materials

Supplementary material associated with this article can be found, in the online version, at doi:10.1016/j.ensm.2023.103029.

References

[1] J. Atik, J.H. Thienenkamp, G. Brunklaus, M. Winter, E. Paillard, Ionic liquid plasticizers comprising solvating cations for lithium metal polymer batteries, Electrochim. Acta 398 (2021), 139333, https://doi.org/10.1016/j.electacta.2021.139333.

[2] J. Atik, D. Diddens, J.H. Thienenkamp, G. Brunklaus, M. Winter, E. Paillard, Cation-assisted lithium ion transport for high performance PEO based ternary solid polymer electrolytes, Angew. Chem. Int. Ed 60 (2021) 11919–11927, https://doi.org/10.1002/anie.202016716.

[3] H.D. Nguyen, G.T. Kim, J. Shi, E. Paillard, P. Judeinstein, S. Lyonnard, D. Bresser, C. Iojoiu, Nanostructured multi-block copolymer single-ion conductors for safer high-performance lithium batteries, Energy Environ. Sci. 11 (2018) 3298–3309, https://doi.org/10.1039/C8EE02093K.

[4] J.-P. Hoffknecht, A. Wettstein, J. Atik, C. Krause, J. Thienenkamp, G. Brunklaus, M. Winter, D. Diddens, A. Heuer, E. Paillard, Coordinating anions "to the Rescue" of the lithium ion mobility in ternary solid polymer electrolytes plasticized with ionic liquids, Adv. Energy Mater. 13 (2023), 2202789, https://doi.org/10.1002/AENM.202202789.

[5] E. Peled, The electrochemical behavior of alkali and alkaline earth metals in nonaqueous battery systems—the solid electrolyte interphase model, J. Electrochem. Soc. 126 (1979) 2047, https://doi.org/10.1149/1.2128859.

[6] S. Menkin, D. Golodnitsky, E. Peled, Artificial solid-electrolyte interphase (SEI) for improved cycleability and safety of lithium-ion cells for EV applications, Electrochem. Commun. 11 (2009) 1789–1791, https://doi.org/10.1016/j.elecom.2009.07.019.

[7] E. Peled, S. Menkin, Review—SEI: past, present and future, J. Electrochem. Soc. 164 (2017) A1703–A1719, https://doi.org/10.1149/2.1441707jes.

[8] R. Shi, Z. Shen, Q. Yue, Y. Zhao, Advances in functional organic material-based interfacial engineering on metal anodes for rechargeable secondary batteries, Nanoscale (2023) 9256–9289, https://doi.org/10.1039/d3nr01306e.

[9] D. Kang, M. Xiao, J.P. Lemmon, Artificial solid-electrolyte interphase for lithium metal batteries, Batter Supercaps 4 (2021) 445–455, https://doi.org/10.1002/batt.202000225.

[10] Y. Zhong, Y. Chen, Y. Cheng, Q. Fan, H. Zhao, H. Shao, Y. Lai, Z. Shi, X. Ke, Z. Guo, Li alginate-based artificial SEI layer for stable lithium metal anodes, ACS Appl. Mater. Interfaces 11 (2019) 37726–37731, https://doi.org/10.1021/ACSAMI.9B12634.

[11] L. Wang, L. Zhang, Q. Wang, W. Li, B. Wu, W. Jia, Y. Wang, J. Li, H. Li, Long lifespan lithium metal anodes enabled by Al_2O_3 sputter coating, Energy Storage Mater 10 (2018) 16–23, https://doi.org/10.1016/J.ENSM.2017.08.001.

[12] W. Beichel, J. Skrotzki, P. Klose, C. Njel, B. Butschke, S. Burger, L. Liu, R. Thomann, Y. Thomann, D. Biro, S. Thiele, I. Krossing, An artificial SEI layer based on an inorganic coordination polymer with self-healing ability for long-lived rechargeable lithium-metal batteries, Batter Supercaps 5 (2022), e202100347, https://doi.org/10.1002/BATT.202100347.

[13] N.-W. Li, Y.-X. Yin, C.-P. Yang, Y.-G. Guo, N.-W. Li, Y.-X. Yin, C.-P. Yang, Y.-G. Guo, An artificial solid electrolyte interphase layer for stable lithium metal anodes, Adv Mater 28 (2016) 1853–1858, https://doi.org/10.1002/ADMA.201504526.

[14] G. Li, S. Liu, Z. Liu, Y. Zhao, High interfacial-energy and Lithiophilic Janus interphase enables stable lithium metal anodes, Small 17 (2021) 1–10, https://doi.org/10.1002/smll.202102196.

[15] D. Lin, Y. Liu, W. Chen, G. Zhou, K. Liu, B. Dunn, Y. Cui, Conformal lithium fluoride protection layer on three-dimensional lithium by nonhazardous gaseous reagent freon, Nano Lett. 17 (2017) 3731–3737, https://doi.org/10.1021/ACS.NANOLETT.7B01020.

[16] K. Park, J.B. Goodenough, Dendrite-suppressed lithium plating from a liquid electrolyte via wetting of Li3N, Adv. Energy Mater. 7 (2017), 1700732, https://doi.org/10.1002/aenm.201700732.

[17] P. Zhao, Y. Feng, T. Li, B. Li, L. Hu, K. Sun, C. Bao, S. Xiong, A. Matic, J. Song, Stable lithium metal anode enabled by high-dimensional lithium deposition through a functional organic substrate, Energy Storage Mater 33 (2020) 158–163, https://doi.org/10.1016/j.ensm.2020.08.025.

[18] D. Kang, N. Hart, J. Koh, L. Ma, W. Liang, J. Xu, S. Sardar, J.P. Lemmon, Rearrange SEI with artificial organic layer for stable lithium metal anode, Energy Storage Mater 24 (2020) 618–625, https://doi.org/10.1016/j.ensm.2019.06.014.

[19] D. Kang, S. Sardar, R. Zhang, H. Noam, J. Chen, L. Ma, W. Liang, C. Shi, J. P. Lemmon, In-situ organic SEI layer for dendrite-free lithium metal anode, Energy Storage Mater 27 (2020) 69–77, https://doi.org/10.1016/j.ensm.2020.01.020.

[20] W. Zhang, S. Zhang, L. Fan, L. Gao, X. Kong, S. Li, J. Li, X. Hong, Y. Lu, Tuning the LUMO energy of an organic interphase to stabilize lithium metal batteries, ACS Energy Lett 4 (2019) 644–650, https://doi.org/10.1021/acsenergylett.8b02483.

[21] J. Wellmann, J.P. Brinkmann, B. Wankmiller, K. Neuhaus, U. Rodehorst, M. R. Hansen, M. Winter, E. Paillard, Effective solid electrolyte interphase formation on lithium metal anodes by mechanochemical modification, ACS Appl. Mater. Interfaces 13 (2021) 34227–34237, https://doi.org/10.1021/acsami.1c07490.

[22] S. Sun, S. Myung, G. Kim, D. Lee, H. Son, M. Jang, E. Park, B. Son, Y.G. Jung, U. Paik, T. Song, Facile ex situ formation of a LiF–polymer composite layer as an artificial SEI layer on Li metal by simple roll-press processing for carbonate electrolyte-based Li metal batteries, J. Mater. Chem. A Mater. 8 (2020) 17229–17237, https://doi.org/10.1039/D0TA05372D.

[23] Y. Liu, R. Hu, D. Zhang, J. Liu, F. Liu, J. Cui, Z. Lin, J. Wu, M. Zhu, Y. Liu, R. Hu, D. Zhang, J. Liu, Z. Lin, M. Zhu, F. Liu, J. Wu, J. Cui, Constructing Li-rich artificial SEI layer in alloy–polymer composite electrolyte to achieve high ionic conductivity for all-solid-state lithium metal batteries, Adv. Mater. 33 (2021), 2004711, https://doi.org/10.1002/ADMA.202004711.

[24] X. Sun, S. Yang, T. Zhang, Y. Shi, L. Dong, G. Ai, D. Li, W. Mao, Regulating Li-ion flux with a high-dielectric hybrid artificial SEI for stable Li metal anodes, Nanoscale 14 (2022) 5033–5043, https://doi.org/10.1039/D2NR01097F.

[25] W. Cao, J. Lu, K. Zhou, G. Sun, J. Zheng, Z. Geng, H. Li, Organic-inorganic composite SEI for a stable Li metal anode by in-situ polymerization, Nano Energy 95 (2022), 106983, https://doi.org/10.1016/J.NANOEN.2022.106983.

[26] Z. Hu, S. Zhang, S. Dong, W. Li, H. Li, G. Cui, L. Chen, Poly(ethyl α-cyanoacrylate)-based artificial solid electrolyte interphase layer for enhanced interface stability of Li metal anodes, Chem Mater 29 (2017) 4682–4689, https://doi.org/10.1021/ACS.CHEMMATER.7B00091.

[27] J. Zeng, Q. Liu, D. Jia, R. Liu, S. Liu, B. Zheng, Y. Zhu, R. Fu, D. Wu, A polymer brush-based robust and flexible single-ion conducting artificial SEI film for fast charging lithium metal batteries, Energy Storage Mater 41 (2021) 697–702, https://doi.org/10.1016/J.ENSM.2021.07.002.

[28] C. Chang, Y. Yao, R. Li, Z.H. Guo, L. Li, C. Pan, W. Hu, X. Pu, Self-healing single-ion-conductive artificial polymeric solid electrolyte interphases for stable lithium metal anodes, Nano Energy 93 (2022), 106871, https://doi.org/10.1016/J.NANOEN.2021.106871.

[29] Z. Yu, D.G. Mackanic, W. Michaels, M. Lee, A. Pei, D. Feng, Q. Zhang, Y. Tsao, C. V. Amanchukwu, X. Yan, H. Wang, S. Chen, K. Liu, J. Kang, J. Qin, Y. Cui, Z. Bao, A. Dynamic, Electrolyte-blocking, and single-ion-conductive network for stable lithium-metal anodes, Joule 3 (2019) 2761–2776, https://doi.org/10.1016/J.JOULE.2019.07.025.

[30] H. Bryngelsson, M. Stjerndahl, T. Gustafsson, K. Edström, How dynamic is the SEI? J. Power Sources 174 (2007) 970–975, https://doi.org/10.1016/j.jpowsour.2007.06.050.

[31] K. Edström, M. Herstedt, D.P. Abraham, A new look at the solid electrolyte interphase on graphite anodes in Li-ion batteries, J. Power Sources 153 (2006) 380–384, https://doi.org/10.1016/J.JPOWSOUR.2005.05.062.

[32] E. Peled, D. Golodnitsky, G. Ardel, Advanced model for solid electrolyte interphase electrodes in liquid and polymer electrolytes, J. Electrochem. Soc. 144 (1997) L208–L210, https://doi.org/10.1149/1.1837858.

[33] Y. Zhou, M. Su, X. Yu, Y. Zhang, J.G. Wang, X. Ren, R. Cao, W. Xu, D.R. Baer, Y. Du, O. Borodin, Y. Wang, X.L. Wang, K. Xu, Z. Xu, C. Wang, Z. Zhu, Real-time mass spectrometric characterization of the solid–electrolyte interphase of a lithium-ion battery, Nat. Nanotechnol. 15 (2020) 224–230, https://doi.org/10.1038/s41565-019-0618-4.

[34] Z. Chen, D. Steinle, H.D. Nguyen, J.K. Kim, A. Mayer, J. Shi, E. Paillard, C. Iojoiu, S. Passerini, D. Bresser, High-energy lithium batteries based on single-ion conducting polymer electrolytes and Li[Ni0.8Co0.1Mn0.1]O2 cathodes, Nano Energy 77 (2020), 105129, https://doi.org/10.1016/j.nanoen.2020.105129.

[35] R. Bouchet, S. Maria, R. Meziane, A. Aboulaich, L. Lienafa, J.-P. Bonnet, T.N. T. Phan, D. Bertin, D. Gigmes, D. Devaux, R. Denoyel, M. Armand, Single-ion BAB

triblock copolymers as highly efficient electrolytes for lithium-metal batteries, Nat. Mater. 12 (2013) 452–457, https://doi.org/10.1038/nmat3602.
[36] L. Porcarelli, A.S. Shaplov, M. Salsamendi, J.R. Nair, Y.S. Vygodskii, D. Mecerreyes, C. Gerbaldi, Single-ion block Copoly(ionic liquid)s as electrolytes for all-solid state lithium batteries, ACS Appl. Mater. Interfaces 8 (2016) 10350–10359, https://doi.org/10.1021/ACSAMI.6B01973.
[37] X. Chen, X. Wang, D. Fang, A review on C1s XPS-spectra for some kinds of carbon materials, Fullerenes Nanotubes Carbon Nanostruct. (2020) 1048–1058, https://doi.org/10.1080/1536383X.2020.1794851.
[38] M. Hekmatfar, A. Kazzazi, G.G. Eshetu, I. Hasa, S. Passerini, Understanding the electrode/electrolyte interface layer on the Li-Rich nickel manganese cobalt layered oxide cathode by XPS, ACS Appl. Mater. Interfaces 11 (2019) 43166–43179, https://doi.org/10.1021/acsami.9b14389.
[39] B. Philippe, R. Dedryvèire, M. Gorgoi, H. Rensmo, D. Gonbeau, K. Edström, Improved performances of nanosilicon electrodes using the salt LiFSI: a photoelectron spectroscopy study, J. Am. Chem. Soc. 135 (2013) 9829–9842, https://doi.org/10.1021/ja403082s.
[40] R. Dedryvère, S. Leroy, H. Martinez, F. Blanchard, D. Lemordant, D. Gonbeau, XPS valence characterization of lithium salts as a tool to study electrode/electrolyte interfaces of Li-ion batteries, J. Phys. Chem. B 110 (2006) 12986–12992, https://doi.org/10.1021/jp061624f.
[41] X. Liu, T. Diemant, A. Mariani, X. Dong, M.E. Di Pietro, A. Mele, S. Passerini, Locally concentrated ionic liquid electrolyte with partially solvating diluent for lithium/sulfurized polyacrylonitrile batteries, Adv. Mater. 34 (2022), https://doi.org/10.1002/adma.202207155.
[42] R. Grissa, V. Fernandez, N. Fairley, J. Hamon, N. Stephant, J. Rolland, R. Bouchet, M. Lecuyer, M. Deschamps, D. Guyomard, P. Moreau, XPS and SEM-EDX study of electrolyte nature effect on li electrode in lithium metal batteries, ACS Appl. Energy Mater. 1 (2018) 5694–5702, https://doi.org/10.1021/acsaem.8b01256.
[43] V. Sharova, A. Moretti, T. Diemant, A. Varzi, R.J. Behm, S. Passerini, Comparative study of imide-based Li salts as electrolyte additives for Li-ion batteries, J. Power Sources 375 (2018) 43–52, https://doi.org/10.1016/j.jpowsour.2017.11.045.
[44] J. Evans, C.A. Vincent, P.G. Bruce, Electrochemical measurement of transference numbers in polymer electrolytes, Polymer (Guildf) 28 (1987) 2324–2328, https://doi.org/10.1016/0032-3861(87)90394-6.
[45] M. Watanabe, S. Nagano, K. Sanui, N. Ogata, Estimation of Li+ transport number in polymer electrolytes by the combination of complex impedance and potentiostatic polarization measurements, Solid State Ion 28–30 (1988) 911–917, https://doi.org/10.1016/0167-2738(88)90303-7.